Reusable Localized Surface Plasmon Sensors Based on Ultrastable Nanostructures**

*Nicolas Vogel, Mathieu Jung, Noelia L. Bocchio, Markus Retsch, Maximilian Kreiter, and Ingo Köper**

***N**anoparticle arrays created by nanosphere lithography are widely used in sensing applications since their localized surface plasmon resonances are extremely sensitive to changes in the local dielectric environment. A major drawback for any biologically oriented sensing application of conventionally produced particle arrays is the lack of stability of the nanoparticles in aqueous media and buffer solutions. Here, a robust and reusable nanoscale sensing platform based on localized surface plasmon resonances of gold nanoparticles embedded in a silicon dioxide matrix is presented. The architecture exhibits extremely high stability in aqueous environments and can be regenerated several times by simple mechanical cleaning of the surface. The platforms surface is ultraflat by design, thus making it an ideal substrate for any bio-oriented sensing application.*

Keywords:
- embedded nanoparticles
- hybrid materials
- localized surface plasmon resonance
- nanosphere lithography
- sensors

1. Introduction

Noble metal nanoparticles have gained increasing attention due to their interesting optical properties[1] and their potential in sensing applications[2,3] or enhanced spectroscopies.[4,5] Collective oscillations of free electrons in a metal particle, known as localized surface plasmon resonances (LSPR) can be excited upon interaction with light of the appropriate wavelength.[3,6,7] The resonance conditions are extremely sensitive to the local dielectric environment of the nanoparticles.[1,8,9] Small changes of the refractive index close to the nanoparticle can cause a shift of the maximum extinction wavelength. This has been exploited in various sensing platforms to detect thin layers of material or binding events of biological species.[3,10–12] These highly versatile and simple platforms can be used for medical diagnostics, drug discovery, or environmental detection of biological agents.[13]

Metal nanoparticles can be produced by various methods, from purely chemical approaches to different lithography techniques.[1] The use of colloidal particles as masks for lithography is a central approach in nanotechnology. It represents an inexpensive, highly parallel, and versatile process that can be used to create large area substrates covered with metal nanostructures.[11,14–16] In particular, nanosphere lithography (NSL)[14–18] has been extensively used to create large highly ordered and uniform arrays of triangular metal nanopyramids by using a densely packed colloidal monolayer as mask.

Previous work has been focused on the detailed examination and on the optimization of the optical properties of particles produced by NSL and other methods.[1,6,11] Furthermore, the response of the optical properties to changes in refractive index of the direct environment of the nanoparticles upon binding events[8,9,12] has been investigated. Significant improvements have been made towards low detection limits, high sensitivity, and spatial resolution in multiplexed assays.[13]

However, conventionally produced nanoparticles suffer from an insufficient stability in aqueous environments.

[*] Dr. I. Köper, N. Vogel, Dr. M. Jung, M. Retsch, Dr. M. Kreiter
Max-Planck-Institute for Polymer Research
Ackermannweg 10, 55128 Mainz (Germany)
E-mail: ingo.koeper@mpip-mainz.mpg.de
Dr. N. L. Bocchio
Laboratoire d'Optique Biomédicale
École Polytechnique Fédérale de Lausanne
1015 Lausanne (Switzerland)

[**] The authors acknowledge Natalie Horn for assistance with SPR measurements and Andreas Unger for the construction of a sample holder. M.R. was sponsored by the Kekulé scholarship provided by the VCI. N.V. acknowledges support from the graduate school *MA*terial Science *IN* Main*Z*.

Supporting Information is available on the WWW under http://www.small-journal.com or from the author.

DOI: 10.1002/smll.200900497

NANO MICRO small

Especially in buffer solutions, commonly used in bioassays, metal nanoparticles tend to be easily washed off the surface.[19] Only recently has this problem started to attract attention and first solutions have been proposed.[20,21] Nanoparticles have been anchored to small holes in the substrates and the decrease in signal intensity over 1 h improved from 50% loss in untreated samples to 13% loss for surface-anchored particles.[20] Recently, highly stable gold structures were obtained by thermal annealing of very thin gold films near the glass transition temperature of the substrate.[21] The gold film separated into individual grains of sizes between 100 and 200 nm that became partly embedded in the substrate. In contrast to NSL, this process did thus not lead to uniform or regular particles.

Next to stability, the reusability of the architecture is important for possible applications, however rarely discussed in literature. Few approaches for regenerating surfaces for surface plasmon resonance experiments on flat metal films[22] or nanoparticle assays[23,24] have been reported, however, no general cleaning methodology has been described. Here, a novel fabrication method has been used to produce large, uniform, and densely packed arrays of surface-embedded metal nanoparticles.[25,26] Their stability upon exposure to commonly used buffer solutions has been probed. Topological and spectroscopic measurements after multiple cycles of material deposition and mechanical removal showed the reusability of the architecture. Such highly stable and reusable platforms should have direct impact both in fundamental research and commercial sensing applications that use metallic nanostructures.

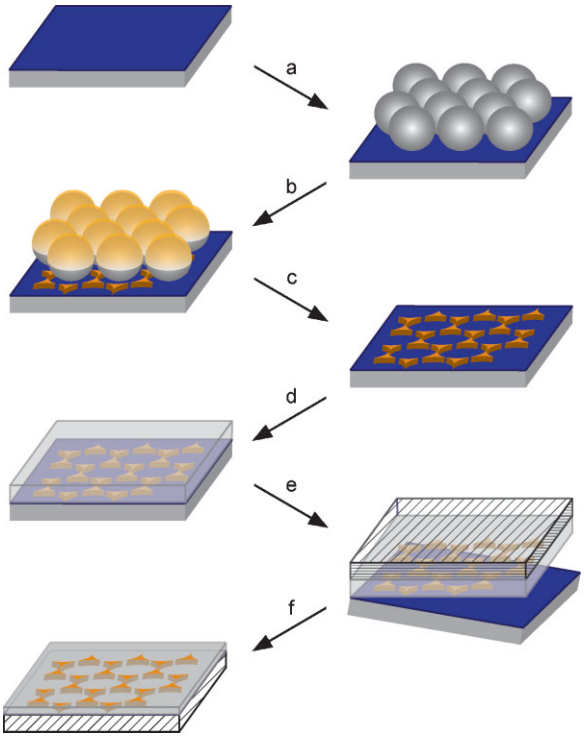

Scheme 1. Flow process for the construction of the embedded nanoparticle arrays. A hexamethyldisilazane-modified wafer is used as template material. a) Colloidal monolayer assembly. b) Thermal evaporation of gold (50 nm) and chromium (<2 nm). c) Removal of the colloidal monolayer. d) Thermal evaporation of silicon dioxide (100 nm). e) Gluing of the interface to a glass slide and mechanical separation. e) Template-stripped surface with gold nanoparticles embedded in a silicon dioxide matrix.

2. Results

2.1. Sample preparation

Large arrays of embedded nanoparticles have been produced using a modified template-stripping[27,28] procedure that allows for the creation of topography-less, patterned substrates (Scheme 1).[25] Briefly, a hexamethyldisilazane-modified silicon wafer was used as a template. A colloidal monolayer was assembled on the template and used as a mask for the deposition of layers of gold (50 nm) and chromium (<2 nm) to produce typical nanopyramid arrays.[15] The colloidal mask was then removed and silicon dioxide (100 nm) was evaporated over the surface and completely covered the patterns. Subsequently, a glass slide was glued onto the silica and a rupture between the passivated template (silicon wafer) and the evaporated structures was mechanically induced. A pristine, flat surface was obtained with gold nanostructure arrays with square-centimeter dimensions embedded in a silicon dioxide matrix (a photograph of a typical sample can be found in the Supporting Information).

Atomic force microscopy (AFM) analysis of the surface showed no topography of the gold nanostructures, which are only vaguely distinguishable from the matrix. During the process, the natural smoothness of the silicon wafer was transferred to the patterned substrate surface and no defect structures between embedded particles and matrix were observable.[25]

2.2. Stability Tests

In order to evaluate the stability of the embedded particle arrays, the substrates were exposed to phosphate buffer solution (PBS) under a constant flow rate of 1.5 mL min^{-1}. The integrity of the samples was followed in time by UV–Vis–NIR transmission spectroscopy (Figure 1a). The obtained extinction data was normalized to the relative peak height ($I_{0,\mathrm{LSPR}}$) before exposure to the aqueous environment (Figure 1b). For comparison, samples of conventionally produced, non-embedded nanoparticles on glass substrates with and without a 2-nm chromium adhesive layer between the glass surface and the gold particles were investigated (Figure 1b). Non-embedded, conventional nanopyramids showed a strong decay in signal intensity. After 20 h of immersion, the extinction decreased to 7.5% of its original value. The sample with a chromium interlayer showed only a slight loss of signal intensity. After several hours, the signal dropped below 90% of the original value. The embedded particles, however, did not show any loss in signal intensity even after 5 days of incubation. Exposure to ultrapure water instead of buffer solution revealed the same stability for the embedded particle arrays (not shown).

To further investigate the stability of the different particle architectures, the chromium-containing samples were cleaned mechanically by wiping the surface with a tissue soaked in water. This drastic procedure revealed a superior robustness of

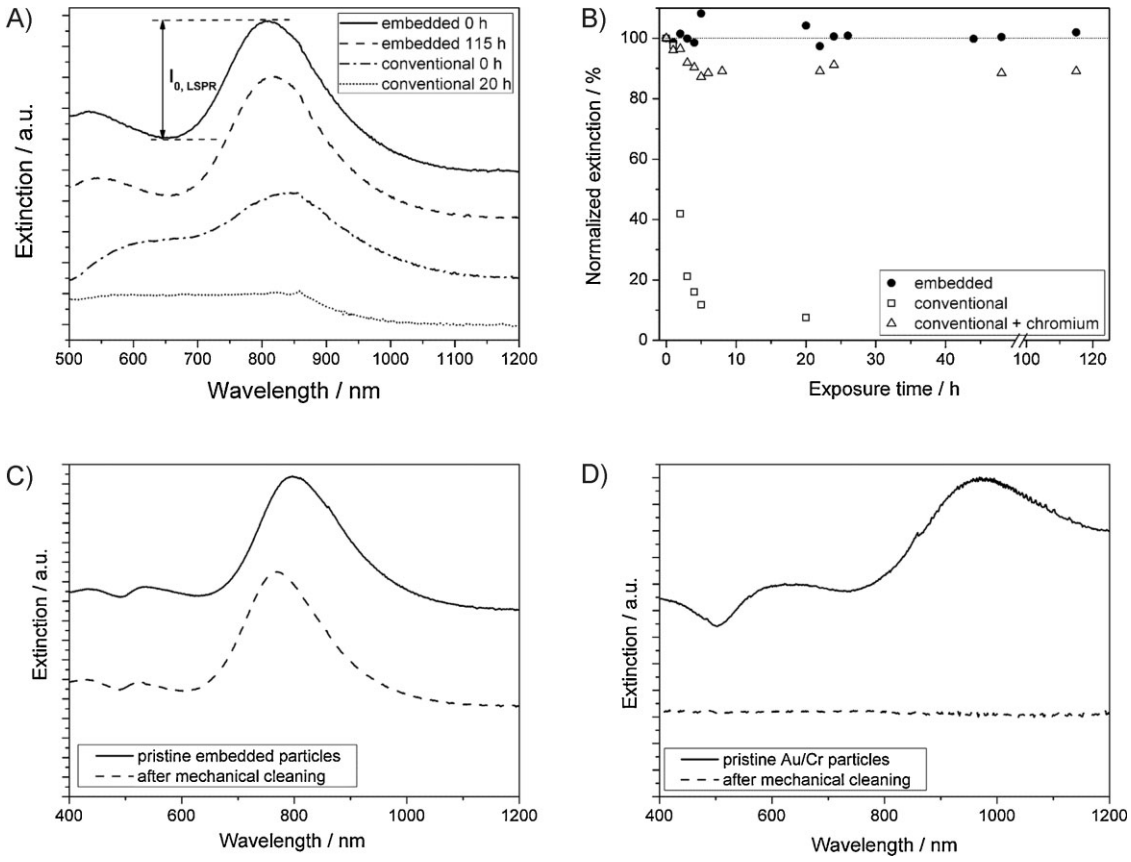

Figure 1. Stability of nanoparticles arrays investigated by UV–Vis–NIR spectroscopy. A) Plasmonic resonances of conventionally produced and surface-embedded nanoparticle arrays upon exposure to PBS. B) Stability of nanoparticle arrays during exposure to PBS normalized to the resonance intensity before exposure. C) Plasmonic resonances of surface-embedded gold particles (50-nm thickness) before and after mechanical cleaning. D) Plasmonic resonances of conventionally produced particles (30-nm thickness) with a 2-nm chromium adhesion layer between glass substrate and gold nanoparticles.

the embedded particles as no change in signal intensity was detected (Figure 1c) after the cleaning. The conventional particle array, however, was entirely removed and no plasmonic resonances were detected (Figure 1d).

2.3. Sensing of Thin Polymeric Layers

In order to probe the response of the embedded particles to changes in their local environment and their potential use for sensing applications, thin polyelectrolyte films were deposited using a layer-by-layer (lbl) deposition method.[29,30] A particle array was produced by using a monolayer of 550-nm-diameter polystyrene colloids as mask. Samples were functionalized by immersion in an aqueous cysteamine hydrochloride solution for 90 min. Afterwards, layers of negatively (poly(styrene sulfonate); PSS) and positively charged (poly(allylamine hydrochloride); PAH) polyelectrolytes were deposited and UV–Vis–NIR spectra were recorded in air. Typical plasmonic resonances were observed (Figure 2a) and a red-shift of the extinction maximum was induced upon increasing the thickness of the deposited polyelectrolyte layers.

The red-shift upon increase in polymer layer thickness can be quantified by extraction of the peak extinction wavelength (Figure 2b). Apart from the shift, no major changes of the plasmon resonance spectra were visible, indicating stability of the particle arrays towards the experimental conditions (see Supporting Information, Figure 2a, for the entire set of spectra). The complete LSPR shift response to material deposition showed a nonlinear behavior as reported for conventionally produced particles.[9] The initial linear shift decreased after the addition of 5–6 bilayers until saturation was reached and no additional shifts of the resonance spectra were detected upon deposition of further layers.

The response of the nanoparticles to the addition of polyelectrolyte layers was estimated from the peak displacement in the initial linear regime. The maximum extinction wavelength shifted on an average by 5.2 nm per deposited layer for the first 6 bilayers (or 12 alternating single layers). The apparent saturation regime after 6 bilayers correlates to a total polyelectrolyte thickness of approximately 50 nm as estimated from SPR spectroscopy measurements on equally treated gold films.[11] The maximum peak displacement between the untreated sample and the one modified with 6 (or more) polyelectrolyte bilayers is about 65 nm, which is in good agreement with results reported for conventionally produced particles.[9] A detailed study of the sensitivity would require to take into account a non-uniform distribution of the polyelectrolyte layers on the substrate caused by the different surface materials[31] as well as an initial non-trivial growth regime of the polyelectrolyte layers,[32] a task that is out of the scope of this work.

NANO MICRO small

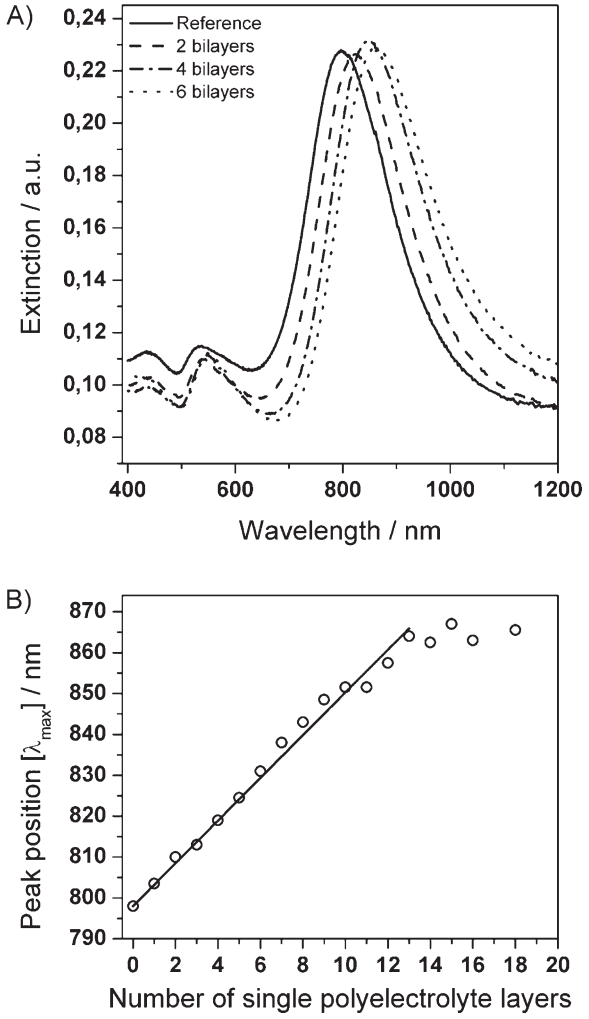

Figure 2. A) Plasmon resonance spectra of the particle array during polyelectrolyte deposition. B) Resonance position as a function of the number of polyelectrolyte layers. The shift is linear for the first 6 deposited layers before an apparent saturation is reached.

2.4. Reusability

The deposited polyelectrolyte layers could be removed by repeated gentle wiping of the substrate with a tissue soaked in ethanol and water. AFM images were recorded in order to monitor the surface during the cleaning process (Figure 3). After cleaning the sample, the original nanostructured surface was completely recovered without any traces of the polyelectrolyte layers remaining on the substrate (Figure 3d). A slight increase in height of the nanostructures can be attributed to the deposited cysteamine layer that is not, or not completely, removed by the mechanical cleaning. However, no damage or loss of structures was induced even by the rather harsh cleaning procedure, showing the stability of the substrates. The cleaned sample was used for further consecutive polyelectrolyte deposition-cleaning cycles to explore the reusability of such a sensing platform. UV–Vis–NIR spectra monitored the effects of the deposition/cleaning cycles on the plasmonic resonances of the embedded nanoparticles (see Supporting Information, Figures 3–5). The peak displacements upon polymer addition evolved similarly to the original sample.

While a blue-shift of the resonances was detected after the first cleaning cycles, no changes in total extinction or sensitivity towards polyelectrolyte binding were apparent for five consecutive deposition/cleaning cycles and the shapes of the resonance spectra remained nearly unaffected by the cleaning procedure (see initial points of the cycles in Figure 4). The origin of the blue-shift of the plasmonic resonance after cleaning is yet not completely clear. It was especially pronounced after the first cleaning step and then decreased until it reached stable values after the fourth cleaning cycle. Additionally, a peak-narrowing of the resonances could be observed. The curves could be described using Lorentzian functions and the half-width-half-maximum (HWHM) values decreased from 130 nm for the first cycle to 100 nm for the fourth cycle (see Supporting Information). Similar to the blue-shift, the HWHM of the curves reached an apparently stable value after the third deposition cycle. Two factors are probably responsible for these phenomena. First, changes in the silicon dioxide layer can cause a blue-shift. The sample was prepared using a thermal evaporation process of silicon dioxide. This is known to result in rather poor quality films.[33,34] Traces of the silicon monoxide precursor or silicon dioxide crystallites that are not fully connected to the matrix might be washed out during the cleaning processes. This would alter the local environment of the particles and lead to a blue-shift of the plasmon resonances. The saturation of the shift to a stable wavelength of 750 nm for the plain nanoparticles after three cleaning cycles supports this assumption. Second, solvent annealing, known to cause blue-shifts in the resonances,[18] can at least partly be responsible for the shift detected in the first measurement cycles. In order to investigate such annealing effects, pristine samples were incubated for 1 h in ethanol and in the electrolyte solutions used as solvents for the polyelectrolytes (an aqueous solution of $MnCl_2$ and HCl as the solvent for the negative polyelectrolyte and NaBr and HCl for the positive polyelectrolyte). While the solvent for the positive polyelectrolyte did not alter the resonances, the incubation in $MnCl_2$-containing negative-polyelectrolyte solution led to a blue-shift in the resonances of about 30 nm (see Supporting Information). Immersion of a sample in ethanol induced a minor blue-shift of about 5 nm after 1 h of incubation. No further changes in the resonances were detected after 23 h of incubation time.

For more quantitative information, the shift of the maximum extinction wavelength was extracted after each deposited layer for a substrate subjected to consecutive lbl deposition/cleaning cycles (Figure 4). For each cycle, at least five polyelectrolyte bilayers were deposited on the surface before the sample was cleaned mechanically. Deposition cycles 4 and 5 were done after storing the substrate for 4 months at lab conditions. For each cycle, the substrate was incubated in a cysteamine solution to guarantee that initial charges are present on the surface. While a red-shift of 5 nm was visible after the assembly of the cysteamine monolayer on the pristine gold surface, almost no shift could be detected for all measurements on cleaned substrates, indicating that the cysteamine layer was not, or not completely, removed by the

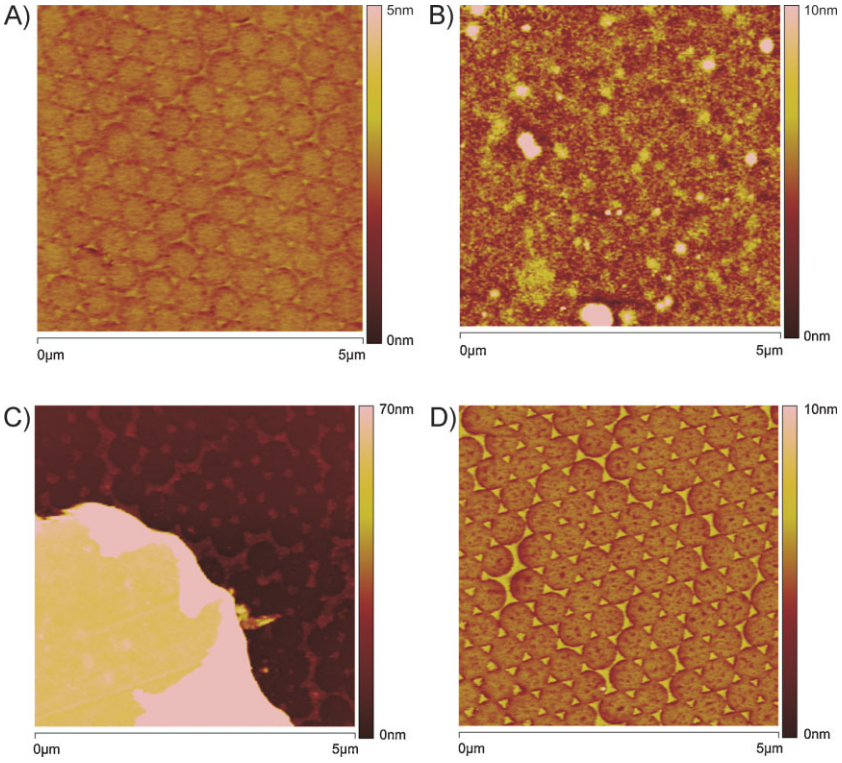

Figure 3. AFM height images of nanoparticle arrays. A) Freshly cleaved substrate. The surface hardly shows any topography. B) After deposition of 8 polyelectrolyte bilayers, the complete substrate is covered with the polymer film. C) The polyelectrolyte film can be mechanically removed. In the lower left corner, a still-intact film is visible, while in the top right corner, the embedded nanostructures become visible. D) On a completely cleaned substrate, the embedded nanoparticles are again visible.

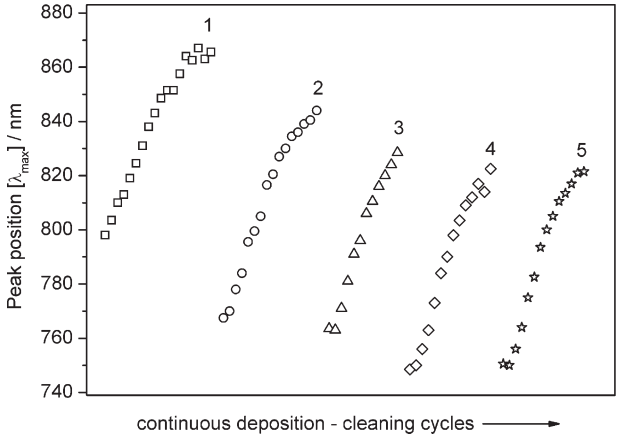

Figure 4. Peak position as a function of the deposition step for 5 consecutive deposition/cleaning cycles. Each symbol (squares, circles, etc.) corresponds to the peak wavelength of the plasmonic resonance after addition of one polyelectrolyte monolayer. Polyelectrolyte layers were added until no further shift in the resonances was visible. Then the polymeric layers were removed by cleaning the surfaces with a tissue soaked in ethanol. The obtained cleaned surface was used for another deposition cycle (indicated by the change of symbols). The first point in each sequence corresponds to the resonance position after cleaning.

cleaning process as also shown by AFM investigation (Figure 3).

For sensing applications, the sensitivity of the plasmonic resonances upon changes in refractive index occurring during binding events on the particles is an important criterion. The maxima of the plasmon resonances red-shifted as a function of deposited layers for all five deposition/cleaning cycles. The slope of the shift curves remained approximately constant at a value of 10–13 nm per bilayer during all cycles, indicating the reusable sensing abilities.

Hence, apart from an initial blue-shift of the resonances after mechanical cleaning, the embedded nanoparticle arrays can be reused multiple times without any significant decrease in signal intensity or sensitivity. The blue-shift may be avoided by the use of a higher quality silicon dioxide matrix (e.g., by a sputtering process) or an initial annealing step using the polyelectrolyte-free solutions.

3. Conclusions

A novel approach to create highly stable nanoparticle arrays is presented. Shifts in the LSPR maximum upon polyelectrolyte deposition showed the sensitivity of the platform for changes in the refractive index of the local environment of the particles. Long-term measurements confirmed the stability of the sensor platforms in buffer solution over extended periods of time. The samples could be cleaned mechanically and consecutive cleaning/deposition cycles did not show any loss in signal intensity or sensitivity, demonstrating the reusability of the nanoparticle-based sensing platform. For potential applications, silicon dioxide can be exchanged for indium tin oxide as matrix material without affecting the construction process[25] in order to electrically address the nanoparticles. This allow the possibility for electrochemical manipulations of the nanostructures, for example, to desorb thiol monolayers or biological materials by an applied voltage.

The inherent ultralow surface roughness[25] of the architecture will have a great advantage for the study of binding events in bio-oriented sensing applications, for example, when using membrane structures assembled on the substrate as sensing matrix, where the membrane formation is crucially influenced by surface roughness.[35]

4. Experimental Section

Sample preparation: Embedded nanoparticle arrays have been produced using a modified template-stripping procedure.[25] In order to passivate the silicon wafer template (CrysTec Kristall-

NANO MICRO small

technologie; Berlin, Germany), a monolayer of hexamethyldisilazane (used as purchased, ABCR Speciality Chemicals; Karlsruhe, Germany) was deposited using vapor phase deposition[36] for 30 min at ambient conditions. The colloidal monolayers used as a mask were prepared by assembly of the colloids at the air–water interface followed by transfer to the substrate.[37] All evaporations were carried out in a Balzers PLS500 evaporation chamber with a Pfeiffer vacuum pump. The pressure in the evaporation chamber was always below 5×10^{-6} mbar before the start of the evaporation process. Gold and chromium were evaporated at a rate of approximately 0.02 nm s^{-1}, silicon monoxide was evaporated at a rate of approximately. 0.1 nm s^{-1} with an oxygen partial pressure of 1×10^{-4} mbar to form the silicon dioxide matrix. All evaporation materials were obtained from Balzers AG (Balzers, Liechtenstein). For gluing, a two-component epoxy glue (EPO TEK 377, Epoxy Technologies; Billerica, USA) was used and cured at 150 °C for 60 min. Before gluing, all glass slides were cleaned by consecutive ultrasonic treatment in 2% detergent solution (Hellmanex; Hellma, Mühlheim, Germany), ultrapure water (Milli-Q; Millipore, Molsheim, France), and ethanol (HPLC grade, Sigma Aldrich; Seelze, Germany). The template-stripping step was performed by carefully scratching on the edges of the silicon wafer glued to the glass slide with a scalpel until the wafer could be lifted off the substrate.

Lbl deposition: The initial cysteamine monolayer was assembled by immersion of the substrate in a 2 mg mL^{-1} solution of cysteamine hydrochloride (Sigma Aldrich; Seelze, Germany) in ultrapure water. Subsequent lbl deposition was performed by immersion for 20 min in solutions of positively and negatively charged polyelectrolytes.

Positively and negatively charged polyelectrolyte solutions: Positively charged solutions were made using 50 mL ultrapure water, 0.0935 g PAH (MW = 15 000), 10.29 g NaBr, and 0.5 mL HCl (0.1 mol L^{-1}). Negatively charged solutions were made using 50 mL ultrapure water, 0.2070 g sodium PSS (MW = 70 000), 4.049 g $MnCl_2$, and 0.5 mL HCl (0.1 mol L^{-1}). All chemicals were obtained from Sigma Aldrich; Seelze, Germany.

Plasmon resonance measurements: Extinction spectra were recorded using a conventional spectrometer (Lambda 900, PerkinElmer). The samples were characterized by AFM on a Dimension 3100 microscope (Veeco Instruments; Plainview, USA) with the Nanoscope version 7.20 software. Silicon cantilevers with a resonance frequency of 300 KHz (Olympus; Tokyo, Japan) were used.

[1] W. A. Murray, W. L. Barnes, *Adv. Mater.* **2007**, *19*, 3771.
[2] P. Englebienne, *Analyst* **1998**, *123*, 1599.
[3] K. A. Willets, R. P. Van Duyne, *Annu. Rev. Phys. Chem.* **2007**, *58*, 267.
[4] S. Kühn, U. Hakanson, L. Rogobete, V. Sandoghdar, *Phys. Rev. Lett.* **2006**, *97*, 17402.
[5] H. Ko, S. Singamaneni, V. V. Tsukruk, *Small* **2008**, *4*, 1980.
[6] T. R. Jensen, M. L. Duval, K. L. Kelly, A. A. Lazarides, G. C. Schatz, R. P. Van Duyne, *J. Phys. Chem. B* **1999**, *103*, 9846.
[7] C. L. Haynes, R. P. Van Duyne, *J. Phys. Chem. B* **2001**, *105*, 5599.
[8] A. J. Haes, S. L. Zou, G. C. Schatz, R. P. Van Duyne, *J. Phys. Chem. B* **2004**, *108*, 6961.
[9] A. J. Haes, S. L. Zou, G. C. Schatz, R. P. Van Duyne, *J. Phys. Chem. B* **2004**, *108*, 109.
[10] W. A. Murray, J. R. Suckling, W. Barnes, *Nano Lett.* **2006**, *6*, 1772.
[11] N. L. Bocchio, A. Unger, M. Alvarez, M. Kreiter, *J. Phys. Chem. C* **2008**, *112*, 14355.
[12] A. J. Haes, R. P. Van Duyne, *J. Am. Chem. Soc.* **2002**, *124*, 10596.
[13] J. N. Anker, W. P. Hall, O. Lyandres, N. C. Shah, J. Zhao, R. P. Van Duyne, *Nat. Mater.* **2008**, *7*, 442.
[14] H. W. Deckman, J. H. Dunsmuir, *Appl. Phys. Lett.* **1982**, *41*, 377.
[15] U. Fischer, H. P. Zingsheim, *J. Vac. Sci. Technol.* **1981**, *19*, 881.
[16] C. L. Haynes, R. P. Van Duyne, *J. Phys. Chem. B* **2001**, *105*, 5599.
[17] J. C. Hulteen, R. P. van Duyne, *J. Vac. Sci. Technol.* **1995**, *13*. 1553.
[18] X. Zhang, A. V. Whitney, J. Zhao, E. M. Hicks, R. P. van Duyne, *J. Nanosci. Nanotechnol.* **2006**, *6*, 1920.
[19] A. J. Haes, J. Zhao, S. Zou, C. S. Owls, L. D. Marks, G. C. Schatz, R. P. van Duyne, *J. Phys. Chem. B* **2005**, *109*, 11158.
[20] E. M. Hicks, O. Lyandres, W. P. Hall, S. Zou, M. R. Glucksberg, R. P. Van Duyne, *J. Phys. Chem. C* **2007**, *111*, 4116.
[21] T. Karakouz, A. B. Tesler, T. A. Bendikov, A. Vaskevich, I. Rubinstein, *Adv. Mater.* **2008**, *20*, 3893.
[22] A. Sato, B. Menges, W. Knoll, *J. Appl. Phys.* **2009**, *105*, 14701.
[23] D. M. Malinsky, K. L. Kelly, G. C. Schatz, R. P. Van Duyne, *J. Am. Chem. Soc.* **2001**, *123*, 1471.
[24] J. C. Riboh, A. J. Haes, A. D. McFarland, C. R. Yonzon, R. P. Van Duyne, *J. Phys. Chem B* **2003**, *107*, 1772.
[25] N. Vogel, M. Jung, M. Retsch, U. Jonas, W. Knoll, I. Köper, *Small* **2009**, *5*, 821.
[26] W. Frey, C. K. Woods, A. Chilkoti, *Adv. Mater.* **2000**, *12*, 1515.
[27] H. J. Butt, D. J. Wang, P. K. Hansma, W. Kühlbrandt, *Ultramicroscopy* **1991**, *36*, 307.
[28] M. Hegner, P. Wagner, G. Semenza, *Surf. Sci.* **1993**, *291*, 39.
[29] G. Decher, *Science* **1997**, *277*, 1232.
[30] G. Decher, J. Schmitt, *Colloid Polym. Sci.* **1992**, *89*, 160.
[31] M. Alvarez, N. L. Bocchio, M. Kreiter, *Langmuir* **2009**, *25*, 1097.
[32] C. C. Buron, C. Filiatre, F. Membrey, C. Bainier, D. Charraut, A. Foissy, *J. Colloid Interface Sci.* **2007**, *314*, 358.
[33] K. Aikawa, H. Sakata, S. Furuuchi, *J. Mater. Sci.* **1978**, *13*, 37.
[34] M. T. K. Soh, N. Savvides, P. J. Martin, C. A. Musca, *Thin Solid Films* **2006**, *515*, 2284.
[35] I. Köper, *Molecular BioSystems*, **2006**, *3*, 651.
[36] U. Jonas, C. Krüger, *J. Supramol. Chem.* **2002**, *2*, 255.
[37] M. Retsch, Z. Zhou, S. Rivera, M. Kappl, X. S. Zhao, U. Jonas, Q. Li, *Macromol. Chem. Phys.* **2009**, *210*, 230.

Received: March 23, 2009
Published online: November 6, 2009

